INTERNATIONAL JOURNAL FOR NUMERICAL METHODS IN FLUIDS
Int. J. Numer. Meth. Fluids 2006; **50**:863–883
Published online 30 September 2005 in Wiley InterScience (www.interscience.wiley.com). DOI: 10.1002/fld.1081

Large eddy simulation of homogeneous shear flows with several subgrid-scale models

Yunliang Wang[1,*,†], Frank G. Jacobitz[2] and Christopher J. Rutland[1]

[1]*Department of Mechanical Engineering, University of Wisconsin—Madison, 1500 Engineering Drive, Madison, WI 53706, U.S.A.*
[2]*Mechanical Engineering Program, University of San Diego, San Diego, CA 92110, U.S.A.*

SUMMARY

In this article, large eddy simulation is used to simulate homogeneous shear flows. The spatial discretization is accomplished by the spectral collocation method and a third-order Runge–Kutta method is used to integrate the time-dependent terms. For the estimation of the subgrid-scale stress tensor, the Smagorinsky model, the dynamic model, the scale-similarity model and the mixed model are used. Their predicting performance for homogeneous shear flow is compared accordingly. The initial Reynolds number varies from 33 to 99 and the initial shear number is 2. Evolution of the turbulent kinetic energy, the growth rate, the anisotropy component and the subgrid-scale dissipation rate is presented. In addition, the performance of several filters is examined. Copyright © 2005 John Wiley & Sons, Ltd.

KEY WORDS: LES; homogeneous shear flow; filter; SGS model

1. INTRODUCTION

Because of the simplicity of homogeneous shear flow and its close relation to geophysical fluid problems, intensive measurements have been carried out in the past decades [1–4]. The experimental data are very useful to validate turbulence models and to determine the model coefficients when a new turbulence model is proposed. Due to the limitation of measurement techniques, however, some important statistical variables such as the dissipation rate of turbulent kinetic energy and higher-order correlation terms are very difficult to measure. For some simple cases, isotropic turbulence, for example, the dissipation rate can be measured using some assumptions. Osborn [5] converted the mean signal shear to the dissipation using the isotropic relation between the shear variance and the dissipation rate. To some extent, this also limits our understanding of the structure of homogeneous shear flow.

*Correspondence to: Yunliang Wang, Department of Mechanical Engineering, University of Wisconsin—Madison, 1500 Engineering Drive, Madison, WI 53706, U.S.A.
†E-mail: ywang@erc.wisc.edu

Received 7 April 2005
Revised 6 August 2005
Accepted 11 August 2005

With the fast development of computer technology and computational fluid dynamics, it has become accessible to solve the instantaneous Navier–Stokes equations directly (direct numerical simulation). Using direct numerical simulation any statistical turbulence variable can be calculated with ease. Rogers and Moin [6] investigated the vorticity structure in a homogeneous turbulent flow using direct numerical simulation. Lee *et al.* [7] carried out direct numerical simulation for a homogeneous turbulent flow with a higher shear rate. The structure of the streaky vorticity and turbulence were studied. Gerz *et al.* [8] performed direct numerical simulations for stratified and unstratified homogeneous shear flows. The effect of buoyancy on the evolution of turbulent kinetic energy and other turbulence variables was examined. With the aid of rapid distortion theory, Rogers [9] investigated the decay of the turbulent kinetic energy in an unstratified shear flow. Holt *et al.* [10] studied the effect of Reynolds number on the evolution of turbulent kinetic energy in a stratified homogeneous turbulent flow. Jacobitz *et al.* [11] carried out direct numerical simulations for stratified homogeneous shear flows. Effects of Reynolds number, shear number and buoyancy were investigated in detail. Jacobitz and Sarkar [12] investigated the effect of non-vertical shear on turbulent homogeneous stratified flows. Kaltenbach *et al.* [13] performed the first large eddy simulation (LES) for stratified homogeneous shear flows. In their simulations, the Smagorinsky model was used to estimate the subgrid-scale (SGS) stress tensor. Since it uses a constant coefficient, the Smagorinsky model has some limitation of application. Numerical simulations have shown that the Smagorinsky coefficient varies with space and time [14]. In addition, the Smagorinsky model cannot handle backscatter transfer due to the positive SGS viscosity. Therefore, more general SGS models such as the dynamic model, the scale-similarity model and the mixed model should be validated intensively. Compared with DNS, LES is more economical numerically since it only resolves the motion of the largest scale. Therefore, with the same grid resolution, LES can deal with flows with much higher Reynolds number. The objective of this study is to examine the performance of several SGS models and filters for homogeneous shear flow. Their performance is validated through the comparison of some estimated turbulence variables with the DNS results. This includes the turbulence kinetic energy, the SGS stresses and the growth rate, etc. Several cases with different initial Reynolds number are studied to explore its effect on the evolution of turbulence for a homogeneous shear flow.

2. MATHEMATICAL PRELIMINARIES

2.1. Mean transport equations

For an incompressible flow, the unsteady three-dimensional Navier–Stokes equations and the transport equation for density can be written as

$$\frac{\partial U_j}{\partial x_j} = 0 \tag{1}$$

$$\varrho\left(\frac{\partial U_i}{\partial t} + U_j\frac{\partial U_i}{\partial x_j}\right) = -\frac{\partial P}{\partial x_i} + \mu\frac{\partial^2 U_i}{\partial x_j \partial x_j} - g\varrho\delta_{i3} \tag{2}$$

$$\frac{\partial \varrho}{\partial t} + U_j\frac{\partial \varrho}{\partial x_j} = \alpha\frac{\partial^2 \varrho}{\partial x_j \partial x_j} \tag{3}$$

Supposing U_i, ϱ and P can be decomposed into a mean part and a fluctuating part, that is

$$U_i = U_i^* + u_i; \quad \varrho = \varrho^* + \rho; \quad P = P^* + p \tag{4}$$

It should be noted that this decomposition is different from the time-based Reynolds decomposition. In this decomposition, the local mean part does not change with time when turbulence is developing. The governing equations can be simplified for flows with mean shear and constant stratification. The flow considered is homogeneous, with constant shear rates in both the vertical and the spanwise directions $\partial U_1^*/\partial x_2 = S_2 = S \sin\theta$ and $\partial U_1^*/\partial x_3 = S_3 = S \cos\theta$, respectively. The mean density has a constant vertical stratification rate $\partial \varrho^*/\partial x_3 = S_\rho$. Then the mean velocity and density can be rewritten in the general forms as

$$U_i^* = (S \sin\theta x_2 + S \cos\theta x_3)\delta_{i1}; \quad \rho^* = \rho_0 + S_\rho x_3 \tag{5}$$

Besides, it is supposed that the mean pressure gradient is balanced by the mean buoyancy force, i.e.

$$\frac{\partial P^*}{\partial x_3} - g(\rho_0 + S_\rho x_3) = 0 \tag{6}$$

This decomposition is introduced into the above equations. Then the following instantaneous equations can be derived:

$$\frac{\partial u_j}{\partial x_j} = 0 \tag{7}$$

$$\frac{\partial u_i}{\partial t} + u_j\frac{\partial u_i}{\partial x_j} + (S \sin\theta x_2 + S \cos\theta x_3)\frac{\partial u_i}{\partial x_1} + (S \sin\theta u_2 + S \cos\theta u_3)\delta_{i1}$$
$$= -\frac{1}{\rho_0}\frac{\partial p}{\partial x_i} + \nu\frac{\partial^2 u_i}{\partial x_j \partial x_j} - \frac{g}{\rho_0}\rho\delta_{i3} \tag{8}$$

$$\frac{\partial \rho}{\partial t} + u_j\frac{\partial \rho}{\partial x_j} + (S \sin\theta x_2 + S \cos\theta x_3)\frac{\partial \rho}{\partial x_1} + S_\rho u_3 = \alpha\frac{\partial^2 \rho}{\partial x_j \partial x_j} \tag{9}$$

In the LES approach, one gets rid of the scales of wavelength smaller than the grid mesh, Δx, by applying an appropriately chosen low-pass filter characterized by the function $\hat{G}$ to the flow to eliminate the fluctuations on SGSs. For any quantity f, the filtered field is defined as

$$\tilde{f}(\mathbf{x}, t) = \int f(\mathbf{y}, t)\tilde{G}(\mathbf{x} - \mathbf{y})\,\mathrm{d}\mathbf{y} = \int f(\mathbf{x} - \mathbf{y}, t)\tilde{G}(\mathbf{y})\,\mathrm{d}\mathbf{y} \tag{10}$$

Employing the above filter to the governing equations, the filtered equations can be written as

$$\frac{\partial \tilde{u}_j}{\partial x_j} = 0 \tag{11}$$

$$\frac{\partial \tilde{u}_i}{\partial t} + \tilde{u}_j\frac{\partial \tilde{u}_i}{\partial x_j} + (S \sin\theta x_2 + S \cos\theta x_3)\frac{\partial \tilde{u}_i}{\partial x_1} + (S \sin\theta \tilde{u}_2 + S \cos\theta \tilde{u}_3)\delta_{i1}$$
$$= -\frac{1}{\rho_0}\frac{\partial \tilde{p}}{\partial x_i} + \nu\frac{\partial^2 \tilde{u}_i}{\partial x_j \partial x_j} - \frac{g}{\rho_0}\tilde{\rho}\delta_{i3} + \frac{\partial \tau_{ij}}{\partial x_j} \tag{12}$$

$$\frac{\partial \tilde{\rho}}{\partial t} + \tilde{u}_j \frac{\partial \tilde{\rho}}{\partial x_j} + (S \sin \theta x_2 + S \cos \theta x_3) \frac{\partial \tilde{\rho}}{\partial x_1} = \alpha \frac{\partial^2 \tilde{\rho}}{\partial x_j \partial x_j} + \frac{\partial q_j}{\partial x_j} - S_\rho \tilde{u}_3 \tag{13}$$

where the SGS stress tensor, τ_{ij}, and the SGS flux, q_j, are given by

$$\tau_{ij} = \tilde{u}_i \tilde{u}_j - \widetilde{u_i u_j}; \quad q_j = \tilde{\rho} \tilde{u}_j - \widetilde{\rho u_j} \tag{14}$$

2.2. *Reynolds-averaged equations*

The transport equation for the Reynolds stresses $R_{ij} = \overline{\tilde{u}_i \tilde{u}_j}$ can be derived from the ith and jth components of the momentum equation.

$$\frac{\mathrm{d}R_{ij}}{\mathrm{d}t} = P_{ij} - B_{ij} + \Pi_{ij} - \varepsilon_{ij} - \varepsilon_{t,ij} \tag{15}$$

where

$$P_{ij} = -S \sin \theta \overline{\tilde{u}_j \tilde{u}_2} \delta_{i1} - S \cos \theta \overline{\tilde{u}_j \tilde{u}_3} \delta_{i1} - S \sin \theta \overline{\tilde{u}_i \tilde{u}_2} \delta_{j1} - S \cos \theta \overline{\tilde{u}_i \tilde{u}_3} \delta_{j1} \tag{16}$$

$$B_{ij} = \frac{g}{\rho_0} (\overline{\tilde{u}_i \tilde{\rho}} \delta_{j3} + \overline{\tilde{u}_j \tilde{\rho}} \delta_{i3}) \tag{17}$$

$$\Pi_{ij} = \frac{1}{\rho_0} \left(\overline{\tilde{p} \frac{\partial \tilde{u}_i}{\partial x_j}} + \overline{\tilde{p} \frac{\partial \tilde{u}_j}{\partial x_i}} \right) \tag{18}$$

$$\varepsilon_{ij} = 2\nu \overline{\frac{\partial \tilde{u}_i}{\partial x_k} \frac{\partial \tilde{u}_j}{\partial x_k}} \tag{19}$$

$$\varepsilon_{t,ij} = \overline{\tau_{ik} \tilde{S}_{jk}} + \overline{\tau_{jk} \tilde{S}_{ik}} \tag{20}$$

The transport equation for the turbulent kinetic energy $K = \overline{\tilde{u}_i \tilde{u}_i}/2$ can be obtained directly from the above equation.

$$\frac{\mathrm{d}}{\mathrm{d}t} K = P - B - \varepsilon - \varepsilon_t \tag{21}$$

where

$$P = -S \sin \theta \overline{\tilde{u}_1 \tilde{u}_2} - S \cos \theta \overline{\tilde{u}_1 \tilde{u}_3} \tag{22}$$

$$B = \frac{g}{\rho_0} \overline{\tilde{u}_3 \tilde{\rho}} \tag{23}$$

$$\varepsilon = \nu \overline{\frac{\partial \tilde{u}_i}{\partial x_k} \frac{\partial \tilde{u}_i}{\partial x_k}} \tag{24}$$

$$\varepsilon_t = \overline{\tau_{ik} \tilde{S}_{ik}} \tag{25}$$

2.3. Definitions of some parameters

The definitions of some parameters used in this study are rewritten here. The characteristic velocity scale, q, is defined by $q=\sqrt{2K}$. The Taylor microscale λ is used, which is calculated by

$$\varepsilon=\frac{10\nu K}{\lambda^2} \tag{26}$$

The corresponding Reynolds number based on λ is defined as

$$Re_\lambda=\frac{q\lambda}{\nu} \tag{27}$$

The shear number is defined as

$$sh=\frac{SK}{\varepsilon} \tag{28}$$

The anisotropy tensor is written as

$$b_{ij}=\frac{\overline{\tilde{u}_i\tilde{u}_j}}{\overline{\tilde{u}_k\tilde{u}_k}}-\frac{1}{3}\delta_{ij} \tag{29}$$

The non-dimensional growth rate γ is defined as

$$\gamma=\frac{1}{SK}\frac{\mathrm{d}K}{\mathrm{d}t}=-2b_{13}\left(1-\frac{\varepsilon}{P}-\frac{\varepsilon_t}{P}-\frac{B}{P}\right) \tag{30}$$

2.4. Numerical approach

In order to use the Fourier models in the spatial discretization, it is necessary to use the period boundary conditions. Due to the effect of mean shear, however, the period boundary conditions cannot be used directly for these equations. To use strictly period boundary conditions, the equations should be transformed into a frame of reference that moves with the mean flow. This approach was originally developed by Rogallo [15]. The following coordinate transformation is used:

$$T=t \tag{31}$$

$$X_i=x_i-Stx_3\delta_{i1} \tag{32}$$

Finally, the transformation leads to the following non-dimensional equations:

$$\frac{\partial\tilde{u}_j}{\partial X_j}-ST\frac{\partial\tilde{u}_3}{\partial X_1}=0 \tag{33}$$

$$\frac{\partial\tilde{u}_i}{\partial T}+u_j\frac{\partial\tilde{u}_i}{\partial X_j}-ST\tilde{u}_3\frac{\partial\tilde{u}_i}{\partial X_1}+S\tilde{u}_3\delta_{i1}=-\frac{1}{\rho_0}\left(\frac{\partial\tilde{p}}{\partial X_i}-ST\frac{\partial\tilde{p}}{\partial X_1}\right)$$
$$-G\tilde{\rho}\delta_{i3}+\frac{\partial\Gamma_{ij}}{\partial X_j}-ST\frac{\partial\Gamma_{i3}}{\partial X_1} \tag{34}$$

where $\Gamma_{ij}=2\nu\tilde{S}_{ij}+\tau_{ij}$ and $\tilde{S}_{ij}=\frac{1}{2}((\partial\tilde{U}_i/\partial X_j)+(\partial\tilde{U}_j/\partial X_i))$.

2.5. Subgrid-scale models

In LES, the most important thing is to estimate the SGS stress tensor in Equation (14). When Boussineq's hypothesis is adopted, the SGS stress tensor and flux become

$$\tau_{ij} = 2\nu_t \tilde{S}_{ij} - \tfrac{1}{3}\tau_{ll}\delta_{ij}; \quad q_j = \alpha_t \frac{\partial \tilde{\varrho}}{\partial x_j} \tag{35}$$

Here, ν_t and α_t are the subgrid eddy viscosity and the subgrid diffusion coefficient, respectively. Usually, α_t is estimated from ν_t via a relation like $\alpha_t = \nu_t / Pr_t$. Here, Pr_t is the SGS Prandtl number. In general, Pr_t is found to increase under stable stratification, which is reflected in different SGS modelling approaches. For example, in the Smagorinsky-type SGS model, the Prandtl number is increased from 0.44 in the free convection limit to 0.7 in neutral condition to 1.0 in the very stable regime [16]. Since we are interested in strongly stable stratification, we adopted the value of unity in our study. Up to date, various SGS models have been proposed. The most widely used model is the Smagorinsky model [17] for the SGS viscosity. It is estimated by

$$\nu_t = C_S^2 (\Delta x)^2 |\tilde{S}| \tag{36}$$

where the shear rate is defined by $|\tilde{S}| = (2\tilde{S}_{ij}\tilde{S}_{ij})^{1/2}$. In the Smagorinsky model, people use various values for C_S, ranging from 0.06 to 0.25 [18, 19]. However, most researchers often adopt the value of 0.1. The selection of C_S depends on the flows encountered. In practical simulations, it is hard to select a reasonable value. To overcome the drawback of choosing C_S, Germano *et al.* [20] developed the dynamic SGS model to calculate the coefficient automatically. Lilly [21] modified the formula for C_S as

$$C_S^2 = \frac{1}{2}\frac{L_{ij}M_{ij}}{M_{ij}M_{ij}} \tag{37}$$

where

$$M_{ij} = \alpha^2 (\Delta x)^2 |\hat{\tilde{S}}| \hat{\tilde{S}}_{ij} - (\Delta x)^2 \widehat{|\tilde{S}|\tilde{S}_{ij}} \tag{38}$$

$$L_{ij} = T_{ij} - \hat{\tau}_{ij} = \hat{\tilde{u}}_i \hat{\tilde{u}}_j - \widehat{\tilde{u}_i \tilde{u}_j} \tag{39}$$

$$T_{ij} = \hat{\tilde{u}}_i \hat{\tilde{u}}_j - \widehat{\widetilde{u_i u_j}} \tag{40}$$

Here, variables under hat symbol ˆ are the filtered values by the test filter of larger grid width $\alpha\Delta x$ (for instance $\alpha = 2$). $|\hat{\tilde{S}}|$ is the filtered shear rate with the test filter defined by

$$|\hat{\tilde{S}}| = \sqrt{2\hat{\tilde{S}}_{ij}\hat{\tilde{S}}_{ij}} \tag{41}$$

Numerical simulations have showed that the coefficient C_S calculated by this form varies significantly with space. Sometimes the variance is as high as 10 times. Besides, some big negative values are frequently encountered, which makes the numerical simulations very unstable. To avoid negative coefficients, most people average the coefficient over the computational domain, or average the numerators and the denominators, respectively [22, 23]. When averaging is used, the dynamic model is no longer so dynamic locally. In addition, when the

Smagorinsky model or the dynamic model is used to calculate the SGS stress tensor, it is found that the predicted stress tensor is very small in comparison with the real SGS stress tensor. Bardina [24] proposed the scale-similarity model to estimate the SGS stress tensor. Bardina's model is written as

$$\tau_{ij} = \hat{\tilde{u}}_i \hat{\tilde{u}}_j - \widehat{\tilde{u}_i \tilde{u}_j} \tag{42}$$

From the analysis of DNS and experimental data, it is found that the scale-similarity model performs very successfully in predicting the real SGS stresses [24, 25]. However, the scale-similarity model does not introduce sufficient dissipation to the turbulent kinetic energy. As a result, some researches combined the scale-similarity model with the Smagorinsky model, or the dynamic model. This is the so-called mixed model.

$$\tau_{ij} = C_{\text{sim}}(\hat{\tilde{u}}_i \hat{\tilde{u}}_j - \widehat{\tilde{u}_i \tilde{u}_j}) + 2C_S^2(\Delta x)^2 |\tilde{S}| \tilde{S}_{ij} \tag{43}$$

where C_{sim} is the coefficient with a value around 1.0. Here, C_S can be a constant or determined by the dynamic model.

2.6. Filters

When the dynamic model or the scale-similarity model is used, a test/second filter is required. The widely used filters are the spectral cut-off filter, Gaussian filter and box filter/top hat filter. The general equation for the discrete filters proposed by Lele [26] is written as

$$\beta \tilde{f}_{i-2} + \alpha \tilde{f}_{i-1} + \tilde{f}_i + \alpha \tilde{f}_{i+1} + \beta \tilde{f}_{i+2} = a f_i + \frac{b}{2}(f_{i+1} + f_{i-1}) + \frac{c}{2}(f_{i+2} + f_{i-2}) + \frac{d}{2}(f_{i+3} + f_{i-3}) \tag{44}$$

When both the values of α and β are zero, the filter is explicit. Otherwise, the filter is implicit or compact. By using different values, we can get the following common filters:

$$\tilde{f}_i = \tfrac{1}{4}(f_{i-1} + 2f_i + f_{i+1}) \tag{45}$$

where $\beta = \alpha = c = d = 0,\ a = b = \frac{1}{2}$.

$$\tilde{f}_i = \tfrac{1}{6}(f_{i-1} + 4f_i + f_{i+1}) \tag{46}$$

where $\beta = \alpha = c = d = 0,\ a = \frac{2}{3},\ b = \frac{1}{3}$.

$$\tilde{f}_i = \tfrac{1}{256}(f_{i-3} - 18f_{i-2} + 63f_{i-1} + 164f_i + 63f_{i+1} - 18f_{i+2} + f_{i+3}) \tag{47}$$

where $\beta = \alpha = 0,\ a = \frac{5}{8},\ b = \frac{63}{128},\ c = -\frac{9}{64},\ d = \frac{1}{128}$.

$$\tfrac{9}{20}\tilde{f}_{i-1} + \tilde{f}_i + \tfrac{9}{20}\tilde{f}_{i+1} = \tfrac{1}{160}(-f_{i-2} + 76f_{i-1} + 154f_i + 76f_{i+1} - f_{i+2}) \tag{48}$$

where $\beta = 0,\ \alpha = \frac{9}{20},\ a = \frac{77}{80},\ b = \frac{19}{20},\ c = -\frac{1}{80},\ d = 0$.

In this study, Equations (45)–(48) are called Filters A, B, C and D, respectively. Filters A and B have second-order truncation accuracy, while, Filters C and D have fourth-order

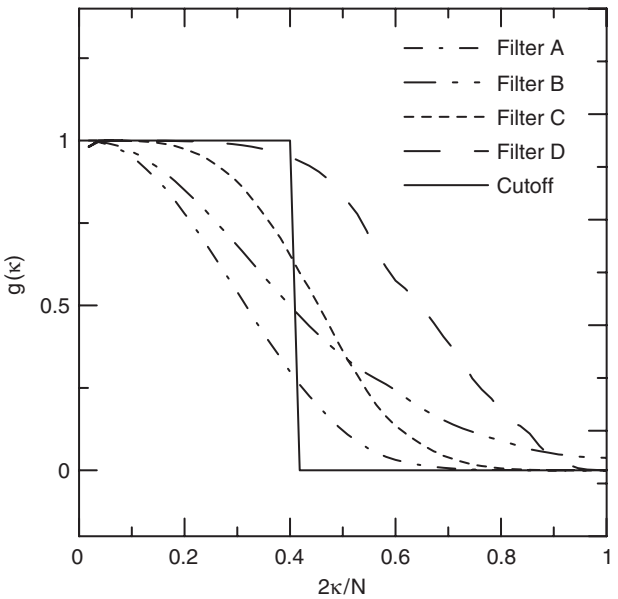

Figure 1. Transfer functions for various filters.

truncation accuracy. Filters A, B and C are the explicit filters, while Filter D is the compact filter. Profiles of the transfer functions for several filters are shown in Figure 1. We can see that Filter D does not filter enough energy for higher wave numbers. Filter A filters too much energy for lower wave numbers. Filter D is close to the cut-off filter for lower wave numbers. For higher wave numbers, however, Filter D cannot filter enough energy necessary for LES. Since Filter C has a higher accuracy and is easy to be applied in practice, Filter C is selected to perform most of the calculations. When the dynamic SGS model is used, we need to calculate the scaling factor $\alpha = \tilde{\Delta}/\Delta$. When the cut-off filter is used, it is straight forward to calculate α using $\alpha = N/k_c$. When the discrete filters are used, we also calculate the cut-off wave number k_c by applying

$$\int_0^{k_c} [1 - g(k)]\,\mathrm{d}k = \int_{k_c}^{N} g(k)\,\mathrm{d}k \tag{49}$$

In this way, the scaling factor can be determined.

3. *A PRIORI* TEST

3.1. Effect of models and filters

To examine the effect of various filters, DNS is carried out with 96^3 grid points for the case of $Re_\lambda = 33$. The SGS stresses and the dissipation rate are calculated from the DNS data by using a filter. In the meantime, four different SGS models are used to calculate these terms. For each SGS model three filters, i.e. the cut-off filter, Filter C and Filter D are tested. Moreover, the SGS stress tensor and the dissipation rate are calculated.

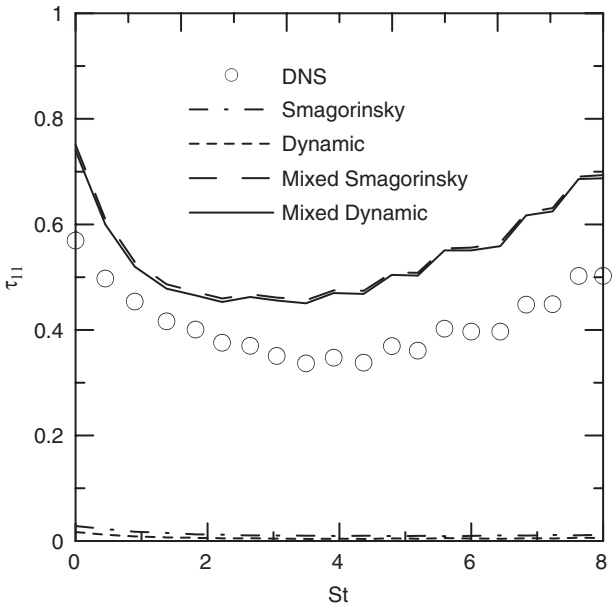

Figure 2. Evolution of τ_{11} with the cut-off filter.

Evolutions of the SGS stress τ_{11} for three filters are plotted in Figures 2–4. These figures show that no matter which filter is used, the mixed Smagorinsky model or the mixed dynamic model performs much better than the Smagorinsky model and/or the dynamic model. This is in agreement with the results of Liu *et al.* [25] for a turbulent jet. Prediction of the Smagorinsky model and the dynamic model is very poor. We also can see that τ_{11} calculated from DNS data using Filter D is smaller than those by Filter C or the cut-off filter. By definition, the SGS stress τ_{11} can be expressed as $\tau_{11} = \int E_{11}(k)[1 - g^2(k)]\,\mathrm{d}k$. Here, E_{11} is the energy spectrum in the x direction and $g(k)$ is the transfer function of the filter. From Figure 1 we can see that $[1 - g^2(k)]$ of Filter D is the lowest. Therefore, τ_{11} by Filter D is smaller than those by Filter C and the cut-off filter. The evolution of other SGS stresses are also examined. Their prediction performance is the same as for the SGS stress τ_{11}.

Evolution of the SGS dissipation rate for the cut-off filter is plotted in Figure 5. Prediction of the Smagorinsky model is closer to the result calculated from the DNS data. Prediction by the dynamic model is smaller than the DNS result. Both the mixed Smagorinsky model and the mixed dynamic model over-predict the SGS dissipation rate. It should be noted that when the cut-off filter is used, we should select two cut-off wave numbers for the filtering, one for the basic filter and the other for the test filter. In Figure 5, the cut-off wave number for the basic filter is N/3 and it is N/4 for the test filter. If the two cut-off wave numbers are set the same, the dissipation introduced by the scale-similarity part is very small, close to zero. Other researchers frequently reported that the SGS dissipation rate is very small when the cut-off filter is used. For example Liu *et al.* [25] did not recommend to use the cut-off filter when the mixed model is used.

Evolution of the SGS dissipation rate for Filter C is shown in Figure 6. Predictions by the Smagorinsky model and the dynamic model are smaller than the DNS data. However, the SGS

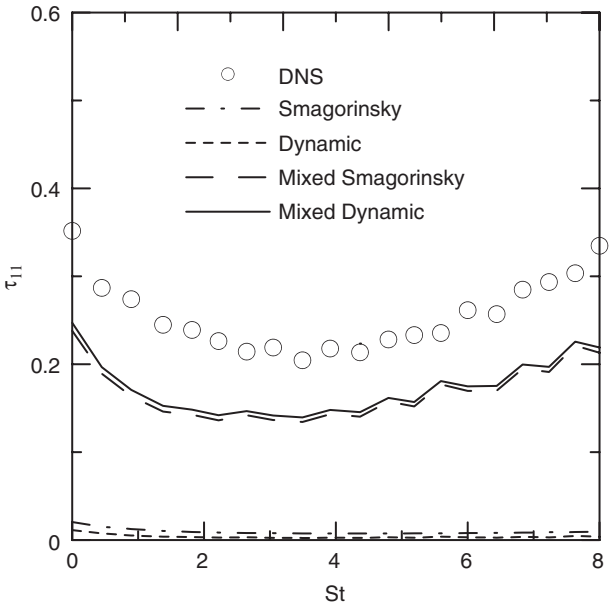

Figure 3. Evolution of τ_{11} with Filter C.

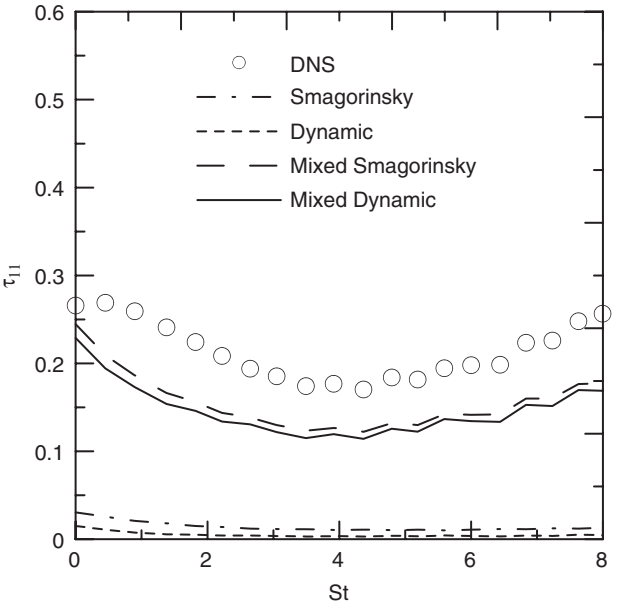

Figure 4. Evolution of τ_{11} with Filter D.

dissipation rate is predicted reasonably by the mixed Smagorinsky model at the beginning. At later times, both the mixed Smagorinsky model and the mixed dynamic model perform better than the other two models. Evolution of the SGS dissipation rate for Filter D is shown in

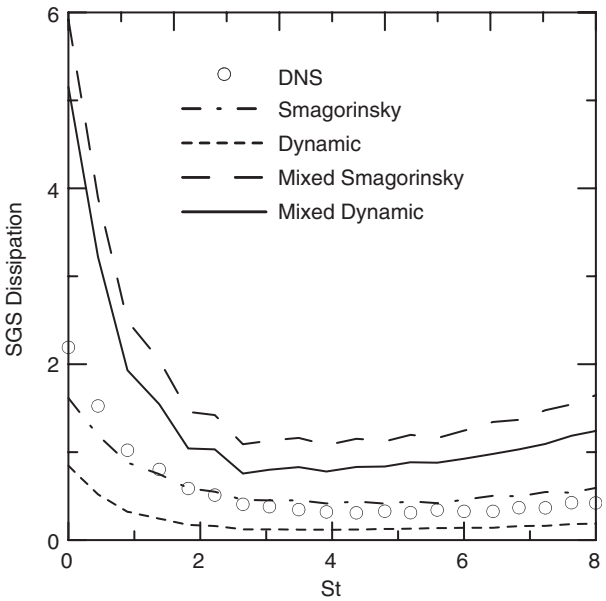

Figure 5. Evolution of SGS dissipation rate with the cut-off filter.

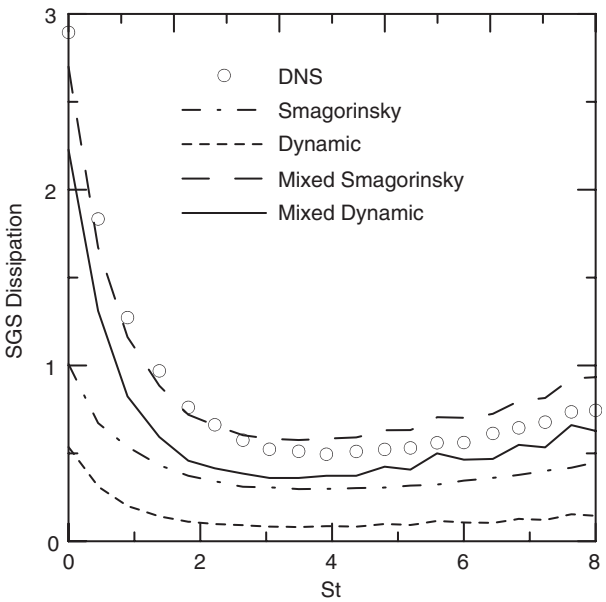

Figure 6. Evolution of SGS dissipation rate with Filter C.

Figure 7. In this case, the Smagorinsky model and the mixed Smagorinsky model over-predict ε_t. The dynamic model under-predicts the dissipation rate. Prediction by the mixed dynamic model is very close to the DNS data. From the above results, it is seen that the overall

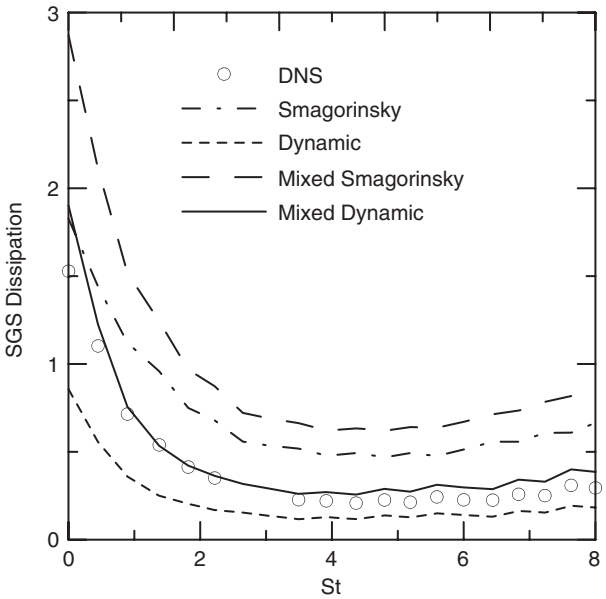

Figure 7. Evolution of SGS dissipation rate with Filter D.

prediction performance of the mixed dynamic model and the mixed Smagorinsky model is better than the other two SGS models. Due to the reason mentioned above, the cut-off filter is not recommended when the mixed model is used. As Filter D is an implicit filter, the tri-diagonal matrix algorithm will be used to calculate the values in each direction, which is very time consuming. Therefore, Filter C is recommended for use with the mixed dynamic model in the following simulations.

4. COMPUTATIONAL RESULTS

4.1. Effect of subgrid-scale models

To investigate the effect of various SGS models, the Smagorinsky model, the scale-similarity model, the dynamic model, the mixed dynamic model and the mixed Smagorinsky model are tested. For the mixed model, both the Smagorinsky model and the dynamic model are used to introduce additional dissipation to the turbulent kinetic energy. The Taylor mircoscale Reynolds number Re_λ is 33. For LES, the grid size should be several times bigger than the Kolmogorov length scale since the smallest scale is not resolved. In the simulation, the ratio of the grid size (0.0654) to the Kolmogorov length scale (0.0132) is 4.95. The shear number SK/ε is 2. In the Smagorinsky model, the Smagorinsky parameter C_S is chosen as 0.1. In the mixed Smagorinsky model, C_S is chosen as 0.08. In the mixed dynamic model, C_S is calculated using the dynamic SGS model. In the mixed model, C_{sim} is chosen as 0.9. Filter C is used in the dynamic SGS model. The scaling factor α in the dynamic SGS model is 2.21 in the simulations. St is the non-dimensional time.

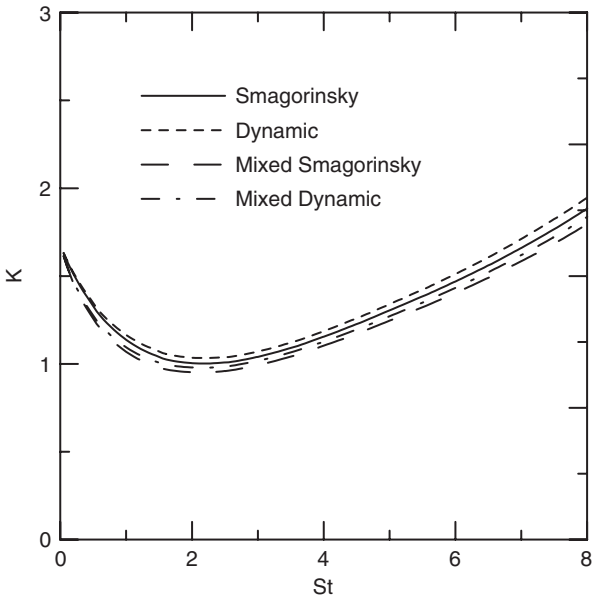

Figure 8. Evolution of the turbulent kinetic energy for the case of $Re_\lambda = 33$.

Evolution of the turbulent kinetic energy is plotted in Figure 8. This figure shows that K decays first and then grows. This is because the initial condition is isotropic and the initial production of the turbulent kinetic energy is zero. It is found that K predicted by the mixed dynamic model and the mixed Smagorinsky model decays faster than those by the dynamic model and the Smagorinsky model at the beginning. The budget of the turbulent kinetic energy for the mixed dynamic model is shown in Figure 9. This figure shows that the dissipation rate of turbulent kinetic energy decreases first, then begins to grow gradually. The production term grows gradually from the isotropic initial state. The sign of $\mathrm{d}K/\mathrm{d}t$ is negative at the beginning since the turbulence decays first. When St reaches the value around 2.3, its sign changes to positive. This means that the production term at this time is already bigger than the total of the turbulent dissipation rate and the SGS dissipation rate. The value of $\mathrm{d}K/\mathrm{d}t$ is in good agreement with the value of $P - \varepsilon - \varepsilon_t$. Although not shown here, the budgets of the turbulent kinetic energy by the other three models show the same tendency as for the mixed dynamic model. One significant difference is the evolution of the SGS dissipation rate by four SGS models as shown in Figure 10. The figure also shows that the SGS dissipation rate ε_t introduced by the dynamic model is smaller than that introduced by the Smagorinsky model. The value of ε_t calculated by both the mixed dynamic model and the mixed Smagorinsky model are larger than that by the dynamic model or the Smagorinsky model. The dynamic model introduces the least SGS dissipation rate of turbulent kinetic energy among the four models.

The evolution of C_S calculated by the dynamic SGS model is shown in Figure 11. The figure shows that C_S decays all the time from the beginning. At the beginning, the value of C_S is around 0.066. This value is smaller than the Smagorinsky coefficient 0.1. However,

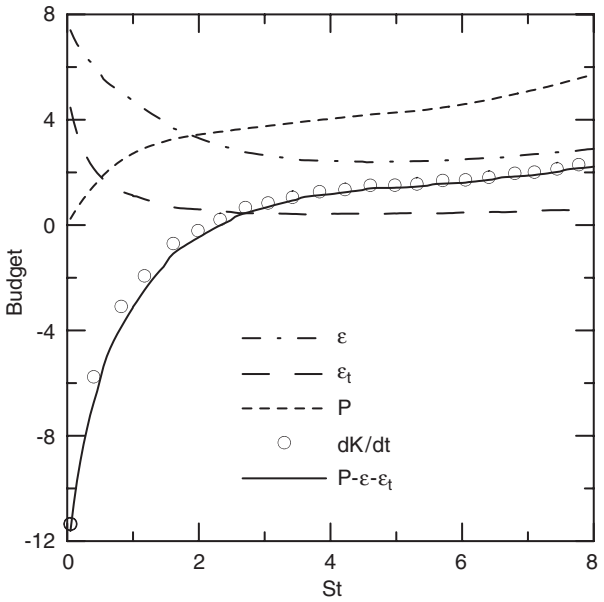

Figure 9. Budget of K equation by the mixed dynamic model.

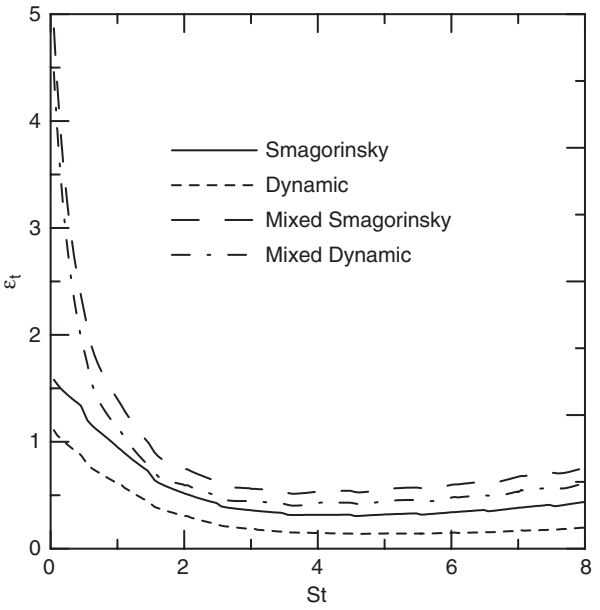

Figure 10. Evolution of ε_t by four SGS models.

it is close to the value 0.06 reported by Piomelli [14]. Therefore, C_S is not only related to space but also to time. Evolution of the SGS viscosity for the case of $Re_\lambda = 33$ is plotted in Figure 12. At the initial, the ratio is about 10.5% for the dynamic model, while it is 15.2% for

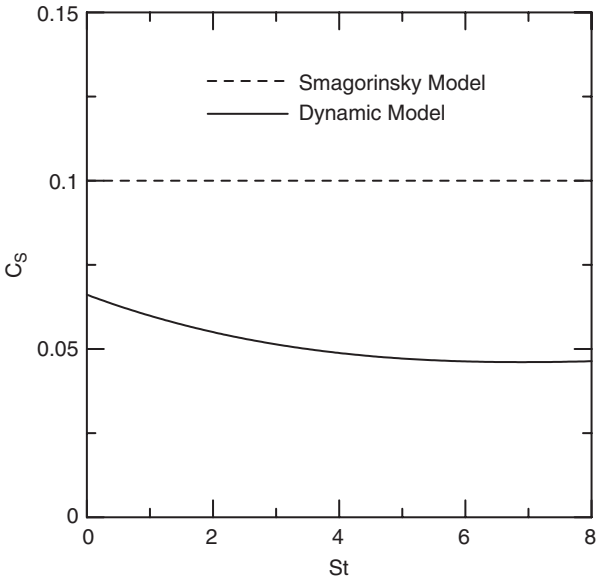

Figure 11. Evolution of C_S by the dynamic model.

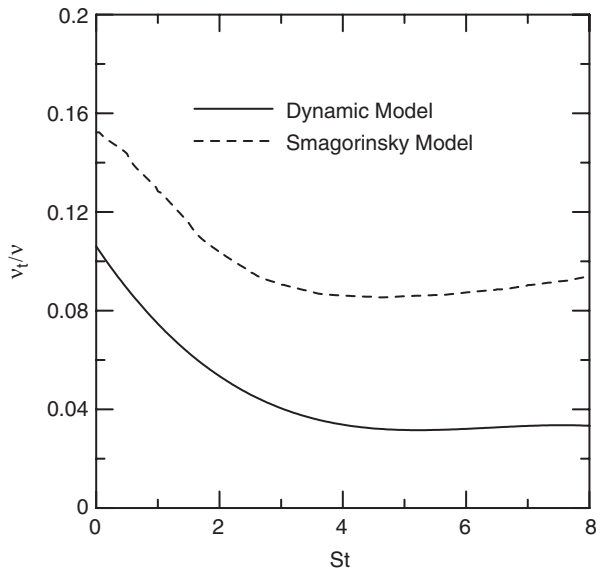

Figure 12. Evolution of ν_t/ν by the dynamic model.

the Smagorinsky model. At $St = 8$, the ratio of ν_t/ν is about 3.5% for the Dynamic model and 9.4% for the Smagorinsky model. Therefore, the SGS viscosity by the Smagorinsky model is usually higher than that by the dynamic model.

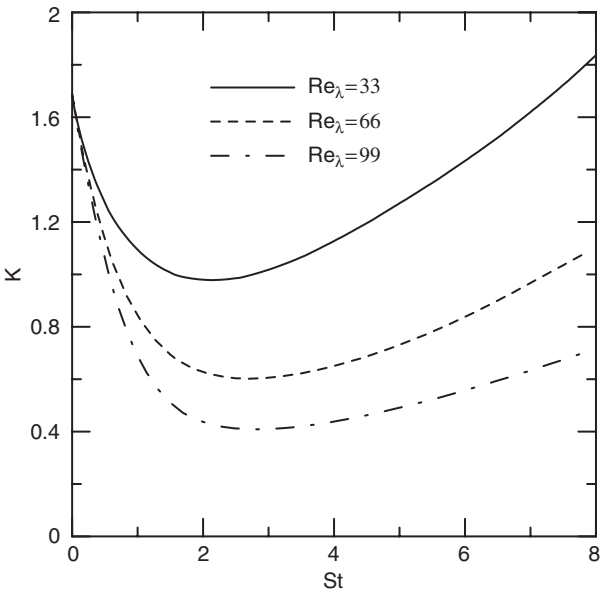

Figure 13. Evolution of K for three initial Reynolds numbers.

4.2. *Effect of Reynolds number*

The effect of Reynolds number is examined in this section. The Reynolds number Re_λ ranges from 33 to 99. The shear number is kept as 2. For the case of $Re_\lambda = 33$, a grid number of 96^3 is used. For other cases, 128^3 grid points are used. The ratio of the grid size to the Kolmogorov length scale is 4.95, 5.44 and 6.66 for $Re_\lambda = 33$, 66 and 99, respectively. The mixed dynamic model is used in all the simulations.

Evolution of the turbulent kinetic energy for three initial Reynolds numbers is plotted in Figure 13. For three initial Reynolds numbers, K decays first and then grows. The evolution of the Reynolds number is shown in Figure 14. It is similar to the evolution of K for three initial Reynolds numbers. With the increase of the Reynolds number, the initial decaying increases. Evolution of the growth rates is shown in Figure 15. At the initial state, the decaying rate increases with the increase of the Reynolds number. Then γ becomes positive, which means K begins to grow. At the final state, γ reaches a maximum and it does not change very much for different Reynolds number. Lohse [27] showed that for $Re_\lambda > 50$, the growth rate should reach an asymptotic value independent of the Reynolds number. Figure 14 shows that the Reynolds numbers at the final state of the simulations lie in the range $62 < Re_\lambda < 116$, therefore, the growth rate is independent of the Reynolds number. Figure 16 shows the evolution of the anisotropy component b_{13} with three initial Reynolds numbers. The absolute value of b_{13} increases from the initial isotropic state. Finally, b_{13} is going to reach an asymptotic value. Figure 17 shows the evolution of the ratio P/ε. With increasing Reynolds number, P/ε decreases at the initial state and finally reaches a value not so dependent on the Reynolds number. It should be pointed out that the tendency of reaching the asymptotic values for b_{13} and P/ε is not so clear since we performed the computations up to $St = 8$. We should have carried out the computations longer.

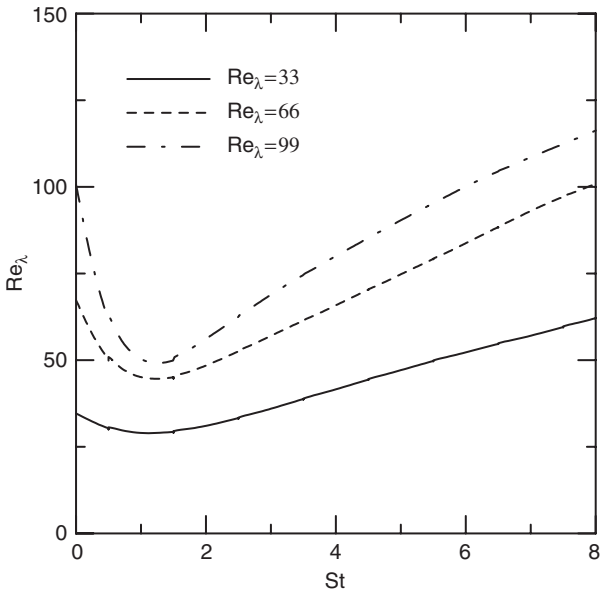

Figure 14. Evolution of the Reynolds numbers.

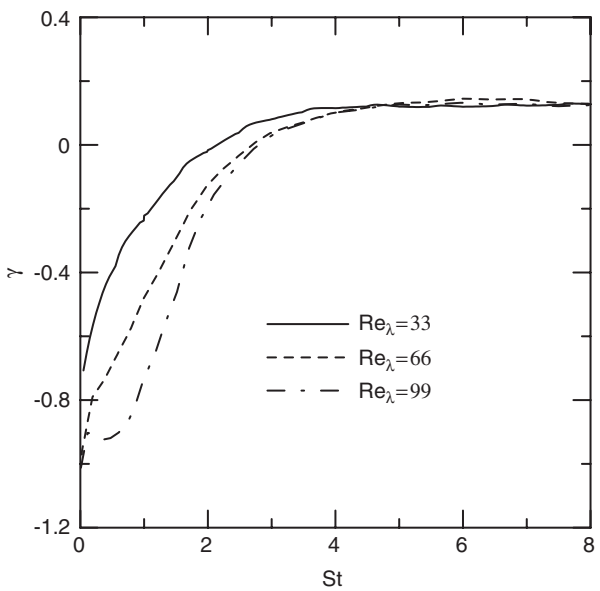

Figure 15. Evolution of the growing rate for three initial Reynolds numbers.

Figure 18 shows evolution of the ratio $\varepsilon_t/\varepsilon$. With the increase in Reynolds number, the ratio becomes higher and higher. At the initial state, the ratio is very high and after $St = 4$, the ratio becomes very flat for the three cases with different Reynolds numbers.

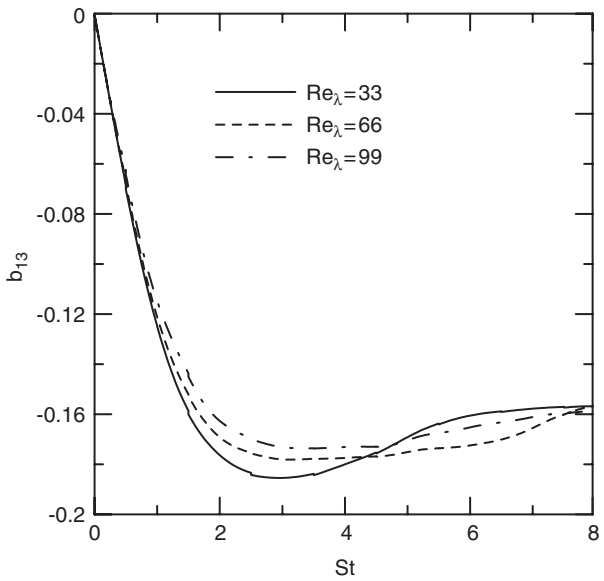

Figure 16. Evolution of b_{13} for three initial Reynolds numbers.

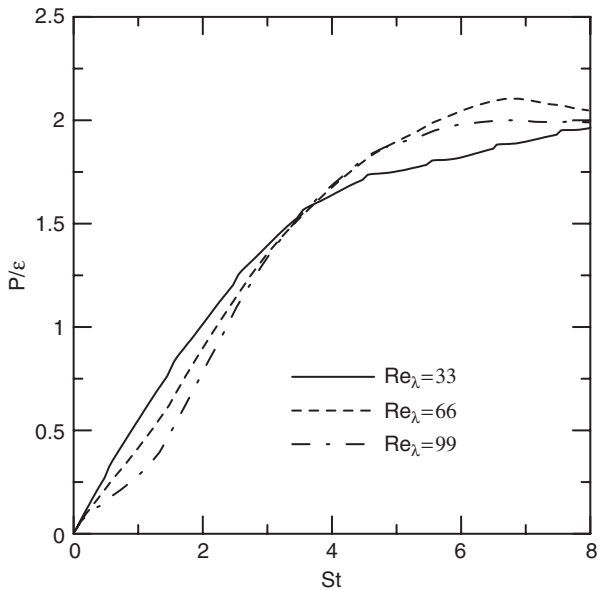

Figure 17. Evolution of P/ε for three initial Reynolds numbers.

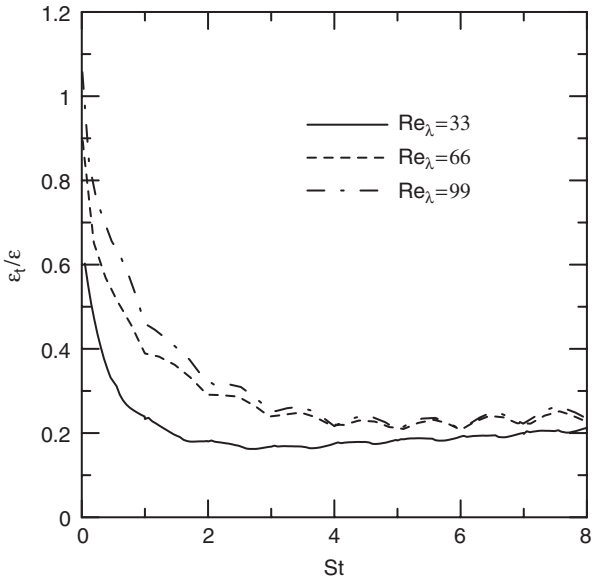

Figure 18. Evolution of $\varepsilon_t/\varepsilon$ for three initial Reynolds numbers.

5. CONCLUSIONS

In this study, large eddy simulations were carried out for the homogeneous shear flow. Evolutions of the turbulent kinetic energy, the anisotropy components, the growth rate, the subgrid-scale viscosity, the subgrid-scale dissipation rate and the budgets of the turbulent kinetic energy equation were presented. The performances of several filters and subgrid-scale models were compared with each other. From the *a priori* test, it is found that the mixed dynamic model and the mixed Smagorinsky model have better overall performance in the prediction of the subgrid-scale stresses and the subgrid-scale dissipation rate than the dynamic model and the Smagorinsky model. When Filter C was used, the mixed Smagorinsky model performs the best among the four models to predict the dissipation rate. When Filter D was used, however, the mixed dynamic model performs the best among the four models in the calculation of the subgrid-scale dissipation rate. From the simulations, it was confirmed that the Smagorinsky parameter C_S is a function of time and space. Therefore, we recommend the use of the mixed dynamic mode rather than the mixed Smagorinsky model, since the mixed dynamic model uses a variable value of C_S rather than a fixed value of 0.1 as used in the Smagorinsky model.

It was also found that the growth rate γ is independent of the Reynolds number when an asymptotic state is reached. The anisotropy component b_{13} and the ratio P/ε need a longer time to reach an asymptotic state. The subgrid-scale dissipation rate increases with the increase of the Reynolds number.

NOMENCLATURE

b_{ij} anisotropy tensor
C_{sim} coefficient

C_S coefficient
g gravity acceleration
$\tilde{G}$ filter function
k_c cut-off wave number
K turbulent kinetic energy
p fluctuating pressure
P total pressure or production term
P^* mean pressure
Pr_t turbulent Prandtl number
q characteristic velocity scale
R_{ij} Reynolds stresses
Re_λ Taylor Reynolds number
sh shear number
S mean shear rate
S_{ij} shear rate tensor
S_ρ vertical stratification
u_i fluctuating velocity components
U_i total velocity components
U_i^* mean velocity components
x_i Cartesian coordinate

Greek letters

α scaling coefficient
α_t subgrid-scale thermal diffusivity
Γ_{ij} total shear stress tensor
Δx grid size
ε dissipation rate of turbulent kinetic energy
ε_t subgrid-scale dissipation rate
η Kolmogorov length scale
θ stratification angle
λ Taylor length scale
μ dynamic molecular viscosity
ν kinematic molecular viscosity
ν_t subgrid-scale eddy viscosity
ρ fluctuating density
ϱ total density
ϱ^* mean density
τ_{ij} subgrid-scale stress tensor

REFERENCES

1. Tavoularis S, Corrsin S. Experiments in nearly homogeneous turbulent shear flow with a uniform mean temperature gradient. *Journal of Fluid Mechanics* 1981; **104**:311–347.
2. Tavoularis S, Karnik U. Further experiments on the evolution of turbulent stresses and scales in uniformly sheared turbulence. *Journal of Fluid Mechanics* 1989; **204**:457–478.
3. Souza FA, de Nguyen VD, Tavoularis S. The structure of highly sheared turbulence. *Journal of Fluid Mechanics* 1995; **303**:155–167.

4. Ferchichi M, Tavoularis S. Reynolds number effects on the fine structure of uniformly sheared turbulence. *Physics of Fluids* 2000; **12**:2942–2953.
5. Osborn TR. Estimates of the local rate of vertical diffusion from dissipation measurements. *Journal of Physical Oceanography* 1980; **120**:83–89.
6. Rogers MM, Moin P. The structure of the vorticity field in homogeneous turbulent flows. *Journal of Fluid Mechanics* 1987; **176**:33–66.
7. Lee MJ, Kim J, Moin P. Structure of turbulence at high shear rate. *Journal of Fluid Mechanics* 1990; **216**: 561–583.
8. Gerz T, Schumann U, Elghobashi SE. Direct numerical simulation of stratified homogeneous turbulent shear flows. *Journal of Fluid Mechanics* 1989; **200**:563–594.
9. Rogers MM. The structure of a passive scalar field with a uniform mean gradient in rapidly sheared homogeneous turbulent flow. *Physics of Fluids A* 1991; **3**:144–154.
10. Holt SE, Koseff JR, Ferziger JH. A numerical study of the evolution and structure of homogeneous stably stratified sheared turbulence. *Journal of Fluid Mechanics* 1992; **237**:499–539.
11. Jacobitz FG, Sarkar S, Van Atta CW. Direct numerical simulations of the turbulence evolution in a uniformly sheared and stably stratified flow. *Journal of Fluid Mechanics* 1997; **342**:231–261.
12. Jacobitz FG, Sarkar S. The effect of non-vertical shear on turbulence in a stably stratified medium. *Physics of Fluids* 1998; **10**:1158–1168.
13. Kaltenbach HJ, Gerz T, Schumann U. Large-eddy simulation of homogeneous turbulence and diffusion in stably stratified shear flow. *Journal of Fluid Mechanics* 1994; **280**:1–40.
14. Piomelli U. High Reynolds number calculations using the dynamic subgrid-scale stress model. *Physics of Fluids A* 1993; **5**:1484–1490.
15. Rogallo RS. Numerical experiments in homogeneous turbulence. *NASA TM 81315*, 1981.
16. Mason PJ, Brown AR. On subgrid models and filter operations in large-eddy simulations. *Journal of the Atmospheric Sciences* 1999; **56**:2101–2114.
17. Smagorinsky J. General circulation experiments with the primitive equations, I. The basic experiment. *Monthly Weather Review* 1963; **91**:99–164.
18. Lesieus M, Metais O. New trends in large-eddy simulations of turbulence. *Annual Review of Fluid Mechanics* 1996; **28**:45–82.
19. Meneveau C, Katz J. Scale-invariance and turbulence models for large-eddy simulation. *Annual Review of Fluid Mechanics* 2000; **32**:1–32.
20. Germano M, Piomelli P, Moin P, Cabot WH. A dynamic subgrid-scale eddy viscosity model. *Physics of Fluids A* 1991; **3**:1760–1765.
21. Lilly DK. A proposed modification of the Germano subgrid-scale closure method. *Physics of Fluids A* 1992; **4**:633–635.
22. Ghosal S, Lund TS, Moin P, Akselvoll K. A dynamic localization model for large eddy simulation of turbulent flow. *Journal of Fluid Mechanics* 1995; **286**:229–255.
23. Meneveau C, Lund T, Cabot W. A Lagrangian dynamic subgrid-scale model of turbulence. *Journal of Fluid Mechanics* 1996; **319**:353–385.
24. Bardina J. Improved subgrid-scale models for large eddy simulation. *AIAA Paper 801357*, 1980.
25. Liu S, Meneveau C, Katz J. On the properties of similarity subgrid-scale models as deduced from measurements in turbulent jet. *Journal of Fluid Mechanics* 1994; **275**:83–119.
26. Lele SK. Compact finite difference schemes with spectral-like resolution. *Journal of Computational Physics* 1992; **103**:16–42.
27. Lohse D. Crossover from high to low Reynolds number turbulence. *Physical Review Letter* 1994; **73**: 3223–3226.

